

Supporting Online Material for **Frictional Afterslip Following the 2005 Nias-Simeulue Earthquake, Sumatra**

Ya-Ju Hsu,* Mark Simons, Jean-Philippe Avouac, John Galetzka, Kerry Sieh, Mohamed Chlieh, Danny Natawidjaja, Linette Prawirodirdjo, Yehuda Bock

*To whom correspondence should be addressed. E-mail: yaru@gps.caltech.edu

Published 30 June 2006, *Science* **312**, 1921 (2006)
DOI: 10.1126/science.1126960

This PDF file includes:

Materials and Methods

Figs. S1 to S10

References

GPS Data

SuGAr cGPS stations recorded data at a 120-second sampling rate and are available from <http://www.tectonics.caltech.edu/sumatra/data>. These data and those from the cGPS station at BAKOSURTANAL's site SAMP near Medan along the northeast coast of Sumatra were processed at Scripps Orbit and Permanent Array Center (SOPAC) using the GAMIT software (1). The data from the SuGAr array were analyzed in 24-hour segments along with the data from 10 additional continuous GPS sites on Java, Cocos Islands, Diego Garcia, Singapore, India, Australia, and Guam. These solutions were combined with global GPS network solutions produced routinely at SOPAC to determine the GPS velocities and displacements and their uncertainties with respect to the ITRF2000 reference frame. Station coordinates are rotated to a reference frame fixed to the Australian plate. All the cGPS data are used as daily positions with typical error at north, east, and vertical components from baseline repeatabilities are 0.31, 0.46 and 0.60 cm, respectively. The coseismic displacements are estimated using the entire available GPS time series for each station and roughly account for interseismic rate and short term postseismic transients. All parameters are estimated simultaneously using least squares.

The Fault geometry and layered model

Our model fault geometry follows the curvature of trench and consists of two segments with dip 10° between 0 km and 20 km depth, and dip 30° between 27 km and 100 km. The Green's functions (2) are calculated using a layered earth model derived from CRUST2.0 (3) sampled at the epicenter. We use a weighted least squares approach with data weights equal to the inverse square root of the data covariance matrix. For the coseismic slip distribution, the relative weight between the GPS and coral data are determined from independent models that use each data set separately. The final model uses both data sets simultaneously, but with the weight of each data set scaled by the

reduced chi-square values inferred from the initial independent models. The rescaling factor between the cGPS data and the coral data is about 7.

In addition, we limit slip directions to be up-dip and right-lateral and consider two different approaches for regularizing the inversions. In the first approach, we minimize the data misfit and model roughness norm. In the second approach, we also minimize the solution length. The relative weights (β , β_1 and β_2 in Fig. S1-S2) between these terms are chosen by cross-validation. In the discussion, we focus on results from the second approach.

Frictional parameters estimated from stress and slip-rate histories

At steady-state sliding, the friction law can be written as $\tau_{ss} = \sigma_n \mu^* + A\sigma_n \log(V/V^*)$, where τ_{ss} is the driving shear stress, σ_n is the normal stress, A is a rheological parameter, presumably positive, V is the sliding velocity, and μ^* and V^* are the reference values (4, 5). Assuming the system is steady-state, then $d\tau_{ss}/d \log V = A\sigma_n$, here τ_{ss} is equivalent to the Coulomb stress change, $\Delta CFS = \Delta\tau - \mu' \Delta\sigma_n$, where $\Delta\tau$ is the shear stress change on the failure plane, μ' is the apparent coefficient of friction including the effect of pore-fluid change, and $\Delta\sigma_n$ is the normal stress change (clamping is positive) (6). We consider a wide range of μ' from 0.2-0.8 and find ΔCFS does not change significantly, since estimated changes in effective normal stress are less than about 20% of shear stress.

Temporal evolution of afterslip

Afterslip can be modeled using a rate- and state-dependent friction law (7). The postseismic displacement resulting from rate-strengthening brittle creep can be written as

$$U(t) = \alpha V_0 t + \beta V_0 t_r \log[1 + d(\exp(t/t_r) - 1)] \quad (\text{S1})$$

where $U(t)$ is the surface displacement, $V_0 = 4 \text{ cm/yr}$ is the interseismic slip rate on the megathrust, α and β are geometric factors, $(\alpha+\beta)V_0$ is the interseismic velocity at the cGPS site, t_r is the relaxation time, and d is the velocity jump due to coseismic stress change. In the single-degree-of-freedom system (7, 8), we have

$$t_r = A\sigma_n / \dot{\tau} \quad (\text{S2})$$

$$d = \exp(\Delta CFS / A\sigma_n) \quad (\text{S3})$$

where A is a rheological parameter, σ_n is the normal stress, $\dot{\tau}$ is the interseismic shear stress rate, and ΔCFS is the co-seismic Coulomb stress change on the creeping patch. The values of t_r and d are determined by least-squares adjustments and equal to about 8 years and 950, respectively. When t is smaller than t_r , equation (S1) simplifies to

$$U(t) \approx \alpha V_0 t + \beta V_0 t_r \log[1 + t / T_{GPS}] \quad (\text{S4})$$

where $T_{GPS} = t_r / d$, is of the order of 3 days. At time larger than about T_{GPS} , postseismic displacements should increase approximately linear with the logarithm of time as observed in this study (Fig. 5 and Fig. S9). The model fits the measured displacements well (Fig. 4A-C, Fig. 5 and Fig. S9), in particular in the early period, where equations S1 or S4 depart from a simple logarithmic dependence on time.

Given that coseismic ΔCFS is of the order of 5 MPa and that the return period of large interplate earthquakes in the area is about 200 years since the penultimate event occurred in 1797, we estimate $\dot{\tau}$ to be about 0.025 MPa/year. Based on the value of t_r and d , and from equations S2 and S3 we estimate $A\sigma_n$ to about 0.2 MPa and 0.7 MPa, respectively.

However, because of the 1-D assumption, the model provides only a crude estimate of the rheological parameters and does not provide much insight into possible spatial variations of the frictional parameters.

Temporal evolution of aftershock

The temporal evolution of aftershocks might reflect the response to the coseismic stress change of the individual secondary faults on which they occur. If these faults are assumed to obey rate-and-state friction with $A < 0$, then the aftershocks sequence would follow approximately the Omori law with the cumulative number of aftershocks increasing as

$$N(t) = N_{t=0} + R_0 t_a \log[1 + d(\exp(t/t_a) - 1)] \quad (\text{S5})$$

where R_0 is the background seismicity rate, t_a is the relaxation time, d expresses the effect of the coseismic stress change ($d = \exp(\Delta CFS / A\sigma_n)$), and $t_a = A\sigma_n / \dot{\tau}$. When t is smaller than t_a , equation (S5) simplifies to

$$N(t) \approx N_{t=0} + R_0 t_a \log[1 + t/T_{as}] \quad (\text{S6})$$

If we assume that the temporal evolution of aftershocks is governed by the time evolution of the stress induced by afterslip (7), such that the delay introduced by the nucleation time of the aftershocks would have a negligible effect. Then the cumulative number of aftershocks should follow the same mathematical equation but with the constraints that T_{as} (equation S6) should be equal to T_{GPS} (equation S4). The cumulative number of aftershocks in the vicinity of the GPS stations seems to vary linearly with postseismic displacement even in the early phase where both departs significantly from a $\log(t)$ dependence (Fig. S9), suggesting that T_{as} and T_{GPS} are of the same order of magnitude.

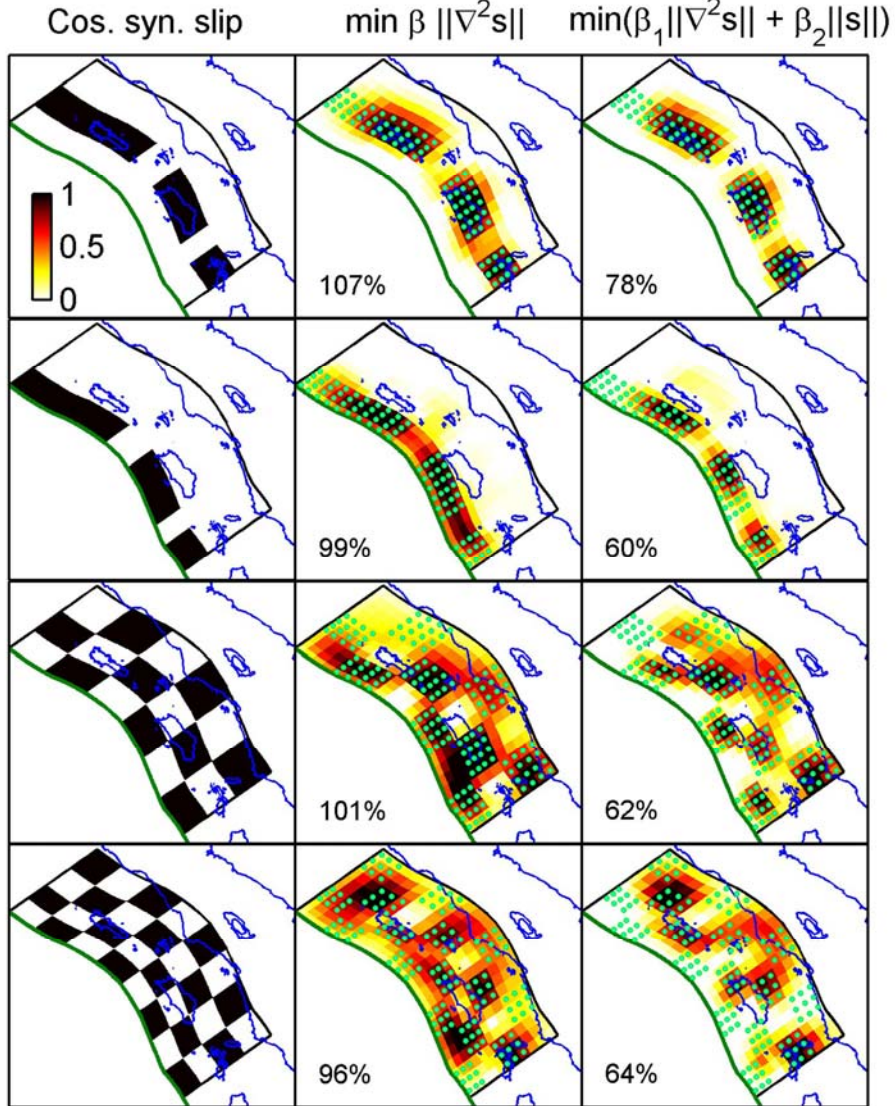


Figure S1 Checkerboard resolution tests using the distribution of observations available for the coseismic model. These tests demonstrate our ability to resolve any up-dip coseismic slip if such slip occurs. The first column shows input models whereby each black rectangle has 1 m of dip-slip. The second and third columns show inversion results with different approaches for regularizing the inversion. We adopt the same data covariance as when using the actual observations. The percentage of the input model potency resolved is indicated in each panel. In the second column we consider models that minimize both data misfit and model roughness with β (damping parameter) equals to 0.025. In the third column, we also minimize the solution length with β_1 and β_2 for the final model equal to 0.017 and 1.4, respectively. Green dots denote the location of 1 m dip-slip in original input model.

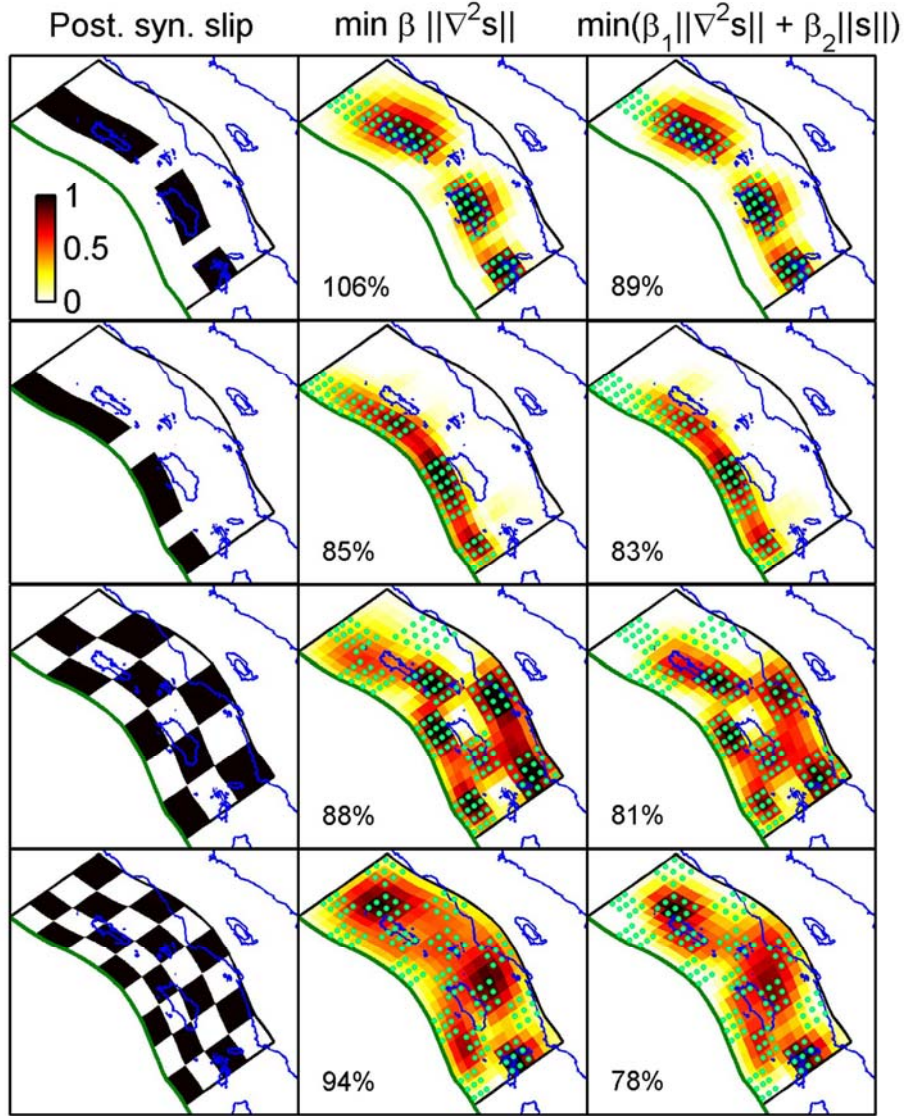


Figure S2. Same as figure S1, but for a data distribution that includes only the available cGPS sites, as is the case for the postseismic models. For synthetic tests in the second column, β equals to 0.028, while in the third column β_1 , β_2 equal 0.02 and 2.5, respectively.

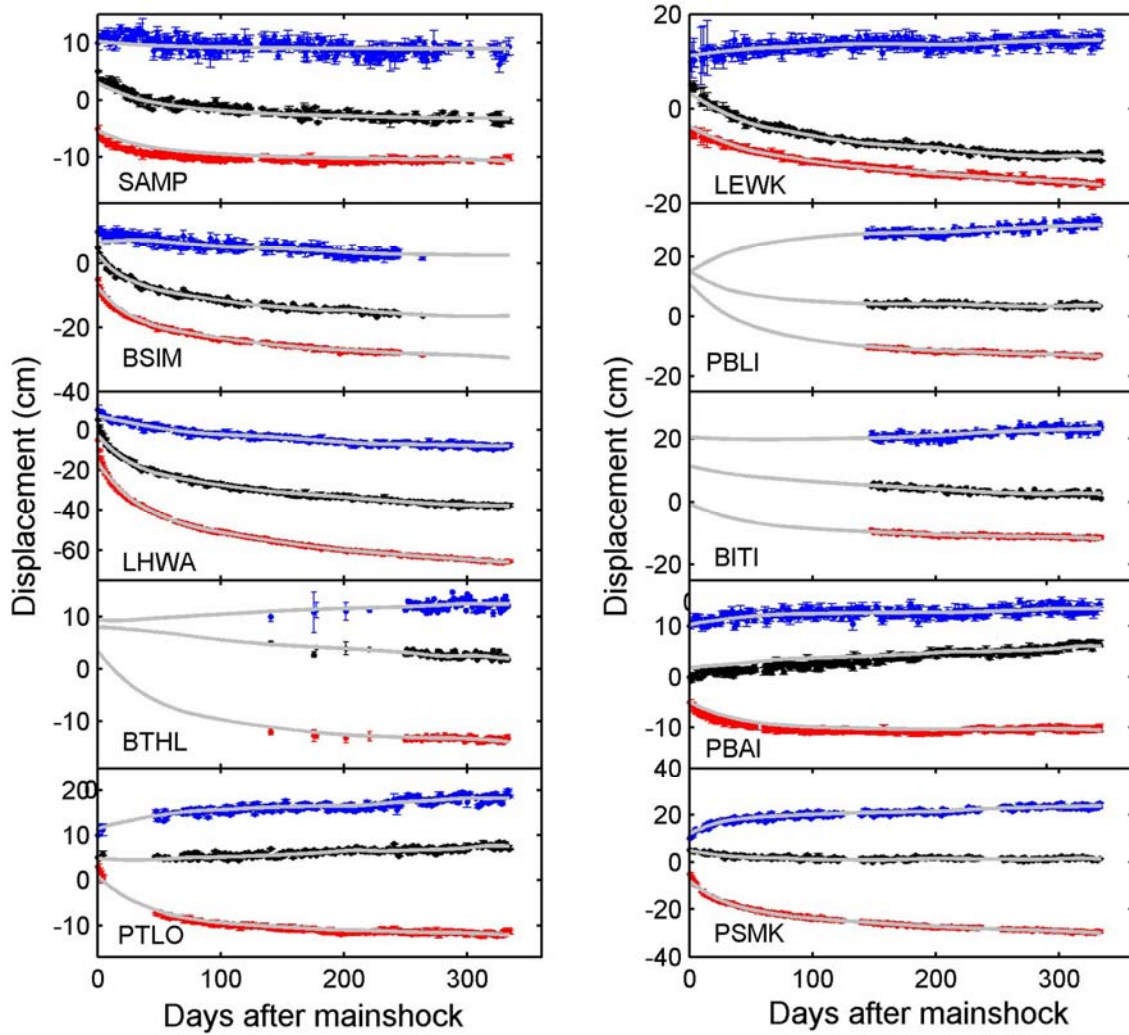


Figure S3 Time series of vertical (U), east (E) and north (N) components of displacement from the cGPS stations used in this study, shown with one sigma error bars. Gray lines indicate predicted displacements from the ENIF time-dependent inversion

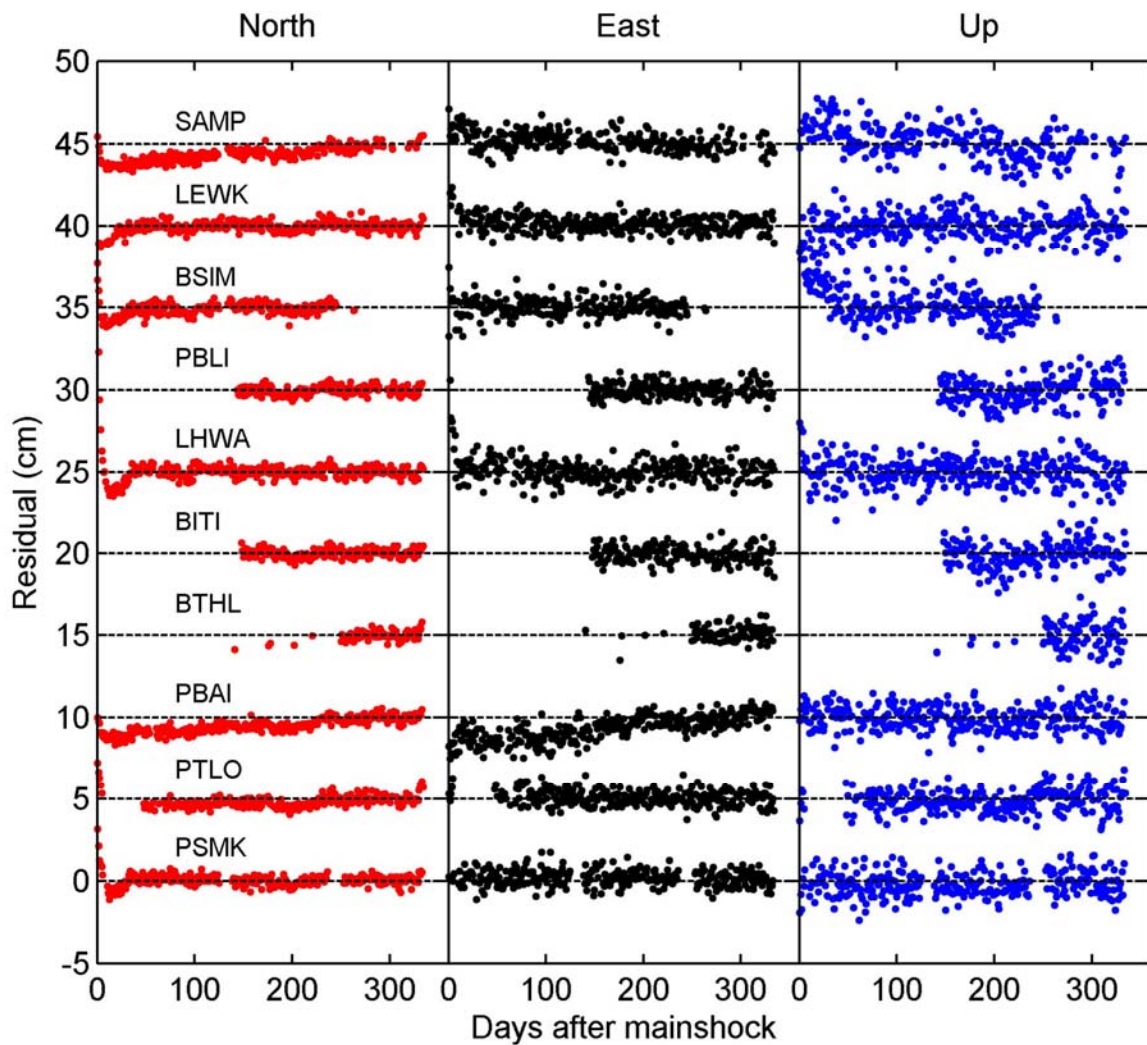


Figure S4 cGPS time-series residuals after removal of the time-dependent afterslip model shown in Fig. S3.

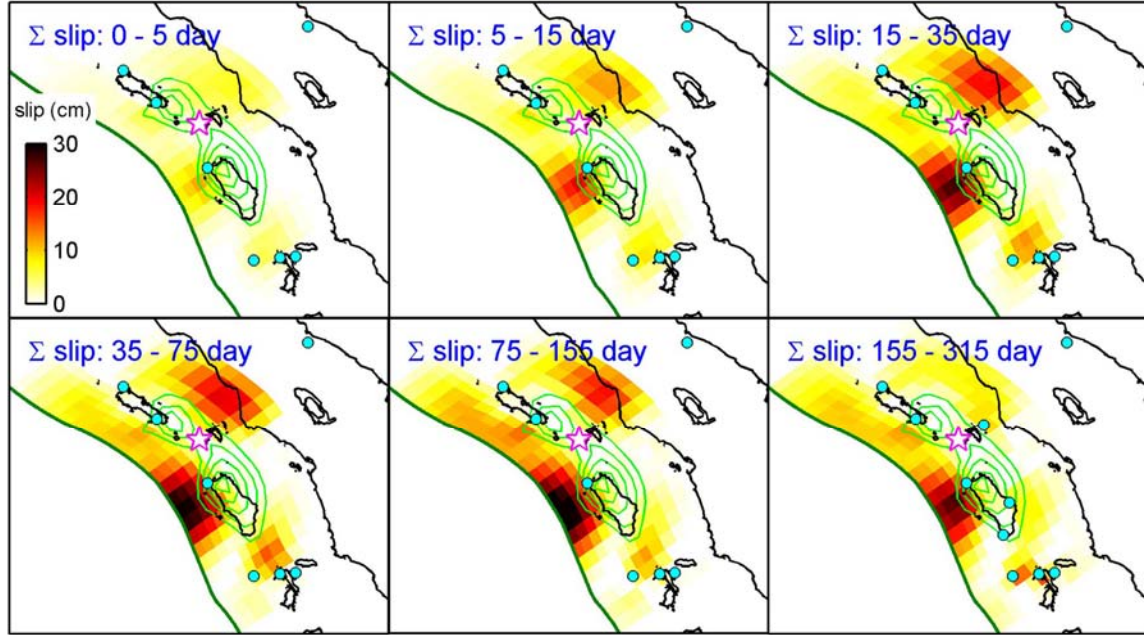


Figure S5. Integrated postseismic slip over consecutive periods of 5, 10, 20, 40, 80, and 160 days. The color scale is cumulative slip for the period specified at top left corner. Green contours show the distribution of coseismic slip at 2 m intervals. The white star denotes the epicenter of Nias-Simeulue earthquake. Blue dots indicate locations of cGPS sites. The regions of inferred afterslip remain fixed, but the relative magnitude of slip varies from one epoch to another.

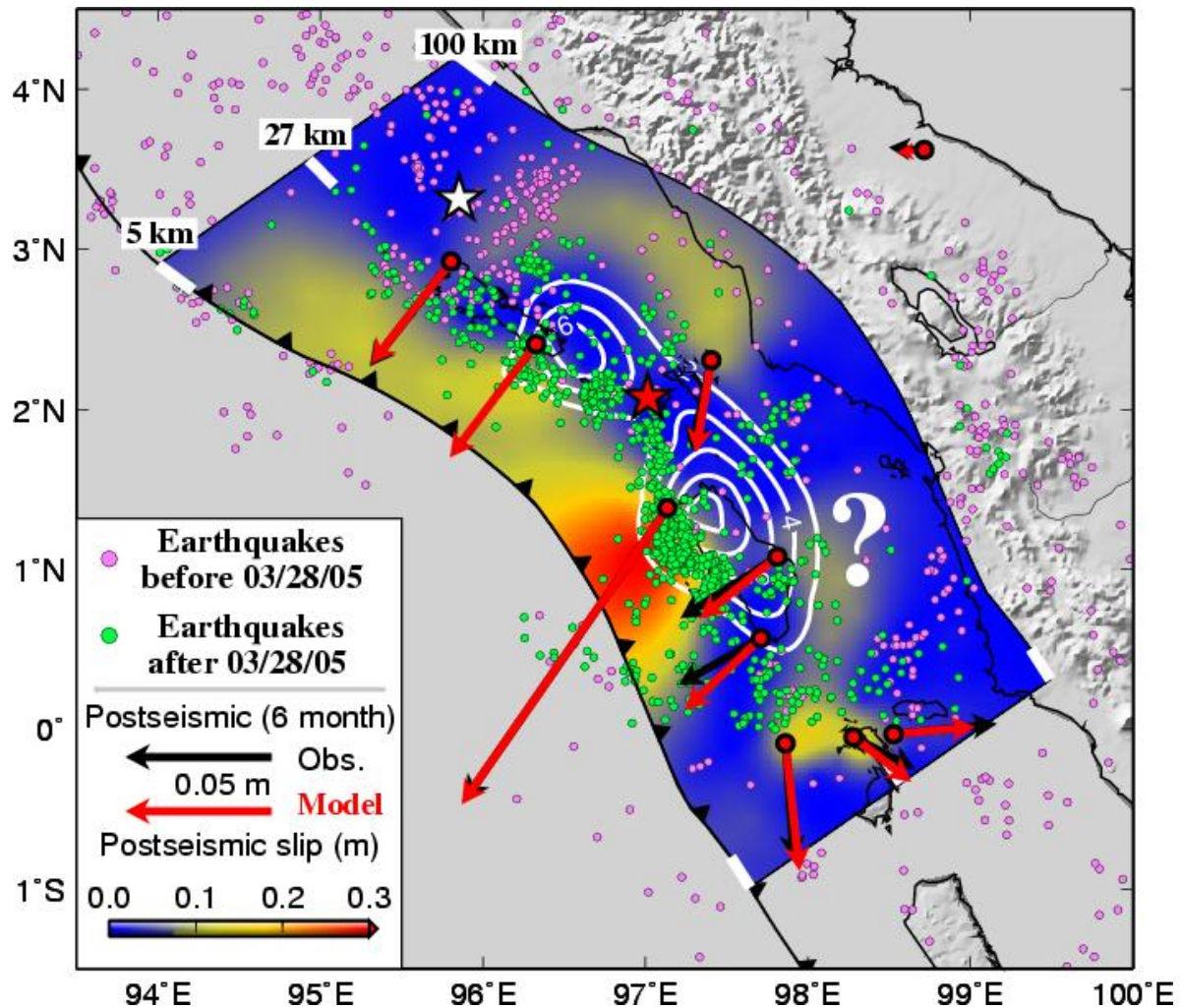


Figure S6 Postseismic slip between 6 months and 11 months after the mainshock is shown in color. For this period, there are 3 more cGPS sites available than in earlier periods. Distribution of coseismic slip indicated by white contours at 2 m interval. Black and red vectors indicate observed and predicted GPS observations. White and red stars are epicenters of 2004 Aceh-Andaman and 2005 Nias-Simeulue earthquakes, respectively. Pink and green dots denote earthquakes with $M_b > 4.5$ before(9) and after (10) 2005 event. The large question mark east of Nias indicates the region where significant afterslip may have occurred at earlier period, but is not detectable with the existing continuous GPS network. White ticks on the northern and southern boundaries of the postseismic slip model indicate depths along the megathrust.

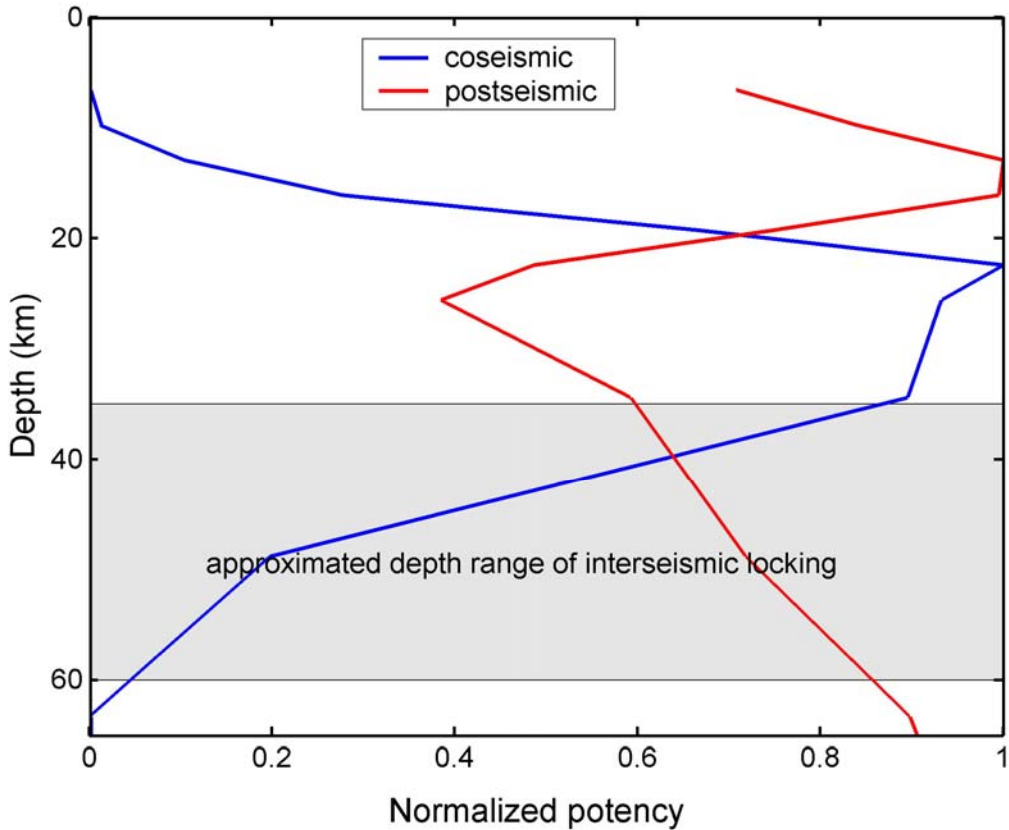


Figure S7 Total potency (product of fault slip and slip area) at a given depth normalized by the maximum value. Blue and red indicate normalized potencies during coseismic and postseismic periods, respectively. The shaded region indicate estimated depth for the transition from stick-slip to stable sliding behavior (11-15).

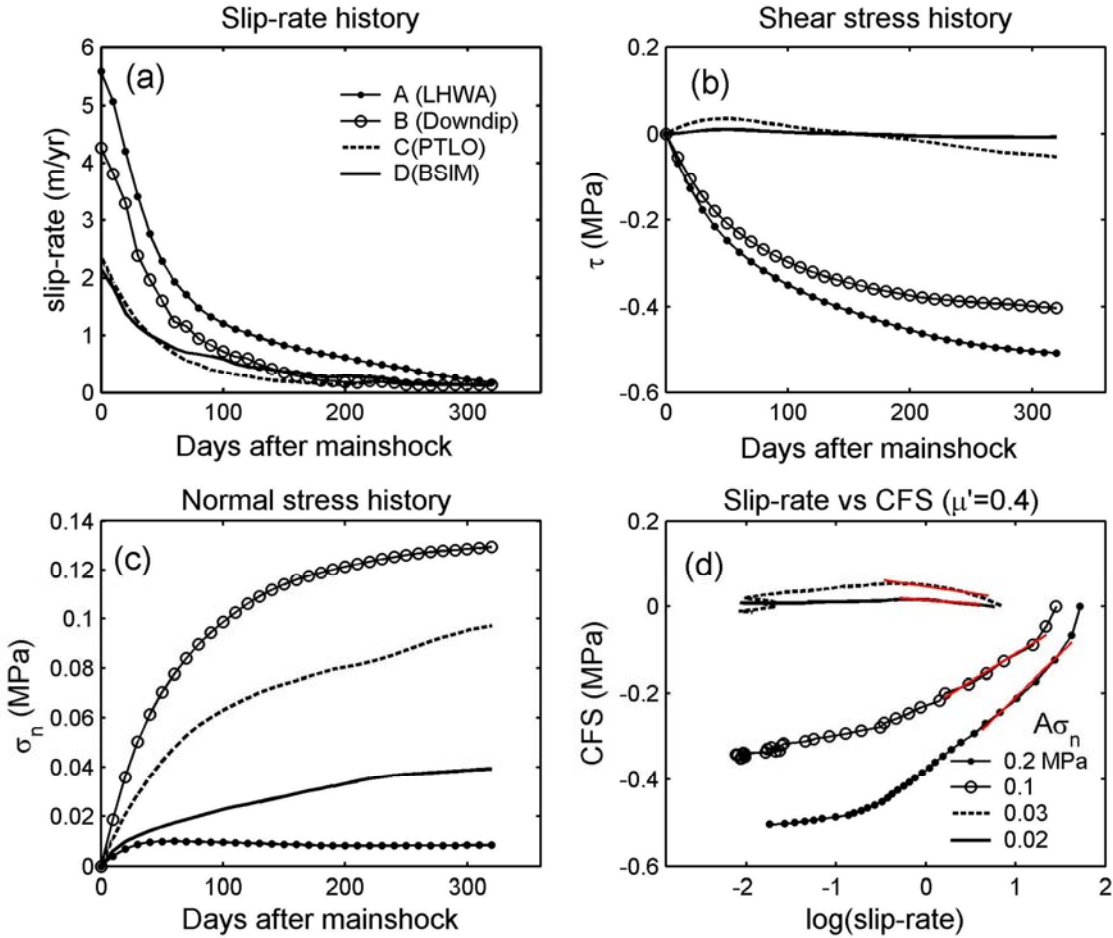


Figure S8 Slip rate (a), shear stress (b), and normal stress (c) histories for four selected areas on the fault (regions shown in Fig. S10). (d) System trajectories in stress change - log (slip-rate) phase space. We use data between 10 days and 2 month after mainshock (red line) to calculate $A\sigma_n$ (values shown at bottom right), where A is a rheological parameter and σ_n is the normal stress.

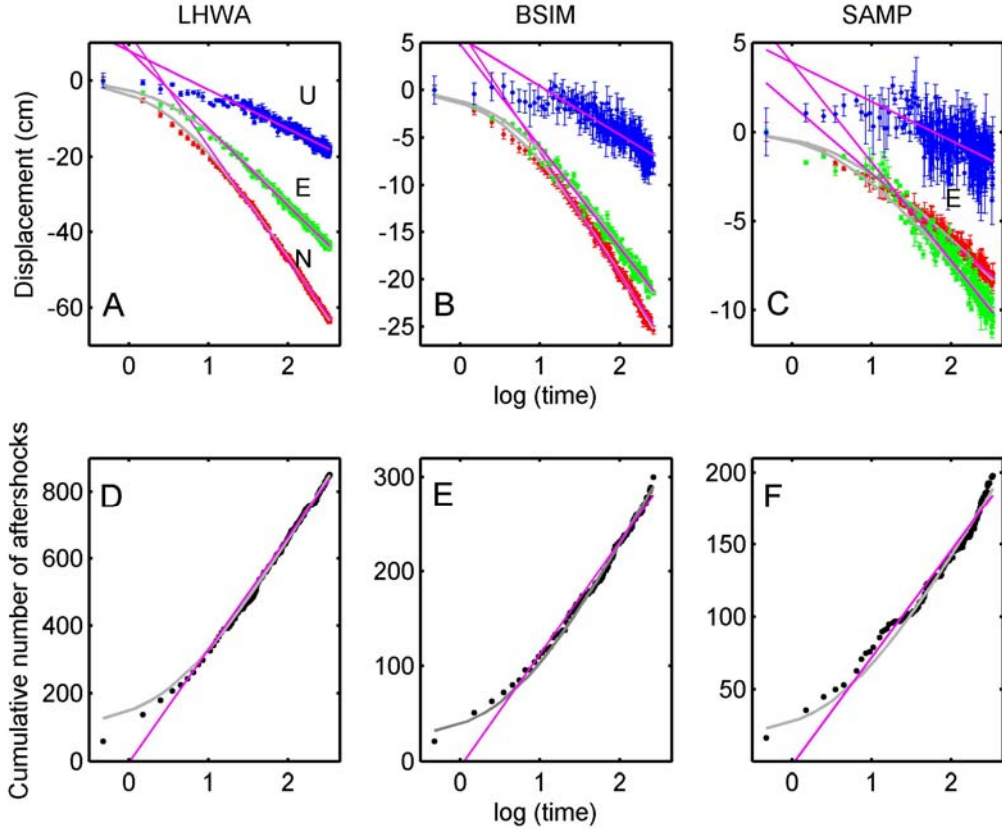


Figure S9 Postseismic displacements and cumulative number of aftershocks as a function of time on linear-log scale. The grey lines in A-C show the predictions of the 1-D rate-strengthening model (equation S1). We compare postseismic displacements at stations LHWA and BSIM, with the aftershocks in their respective vicinity (Fig. S10, black box), located at the down-dip end of shallow afterslip. We also compare postseismic displacements at SAMP with the deeper band of aftershocks. Aftershocks with magnitude larger than 3 are obtained from IRIS (2005/03/28-2006/02/24), presumably above the magnitude of completion of that catalogue for this area (10). The time evolution of aftershocks for all three areas (grey lines in D-F) follows reasonably well the predictions of equation S5 with constraints that the t_a and d be the same as t_r and d estimated from the fit of equation S1 to the postseismic displacements. Pink lines denote roughly linear variations of postseismic displacement and cumulative number of aftershocks with the logarithm of time when $t \gg T_{GPS}$ (equation S4).

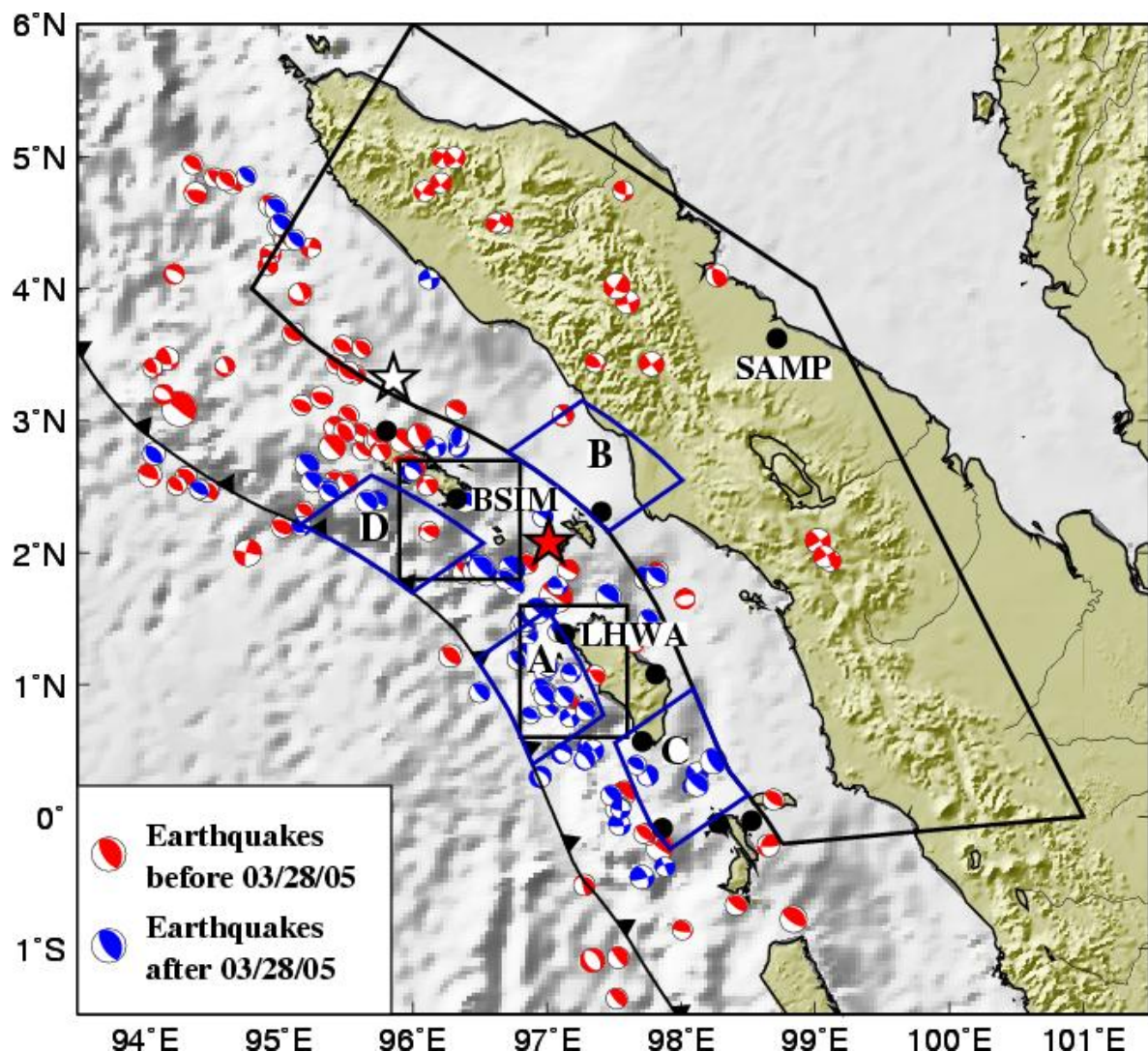


Figure S10 Earthquake focal mechanisms from the Harvard CMT catalog for the period 1980 to 2005 with $M_w > 4.5$ and depth < 100 km (16). Red and blue focal mechanisms indicate earthquakes before and after the 2005 Nias-Simeulue earthquake, respectively. Black boxes indicate regions used for counting the cumulative number of aftershocks in Fig. 4. Blue boxes denote the region used for estimating slip and stress histories in Fig. S8.

Supporting Online Material: References

- S1. R. King, Y. Bock, Mass. Inst. of Technol., Cambridge, Mass. and Scripps Inst. of Oceanogr., La Jolla, Calif. (2000).
- S2. Y. H. Zeng, *Geophys. Res. Lett.*, **28**, 3007 (2001).
- S3. C. Bassin, G. Laske, G. Masters, *EOS Trans AGU*, F897 (2000).
- S4. J. H. Dieterich, *J. Geophys. Res.*, **84**, 2161 (1979).
- S5. A. Ruina, *J. Geophys. Res.*, **88**, 359 (1983).
- S6. G. C. P. King, R. S. Stein, J. Lin, *Bull. Seismol. Soc. Am.*, **84**, 935 (1994).
- S7. H. Perfettini, J. P. Avouac, *J. Geophys. Res.*, **109**, doi:10.1029/2003JB002917 (2004).
- S8. H. Perfettini, J. P. Avouac, *J. Geophys. Res.*, **109**, doi:10.1029/2003JB002488 (2004).
- S9. E. R. Engdahl, A. Villaseñor, H. R. DeShon, *Bull. Seismol. Soc. Am.*, in press.
- S10. Seismicity obtained from Incorporated Research Institutions for Seismology (IRIS) at <http://www.iris.washington.edu/SeismiQuery/events.htm>
- S11. M. Chlieh *et al.*, AGU Fall Meeting, Abstract A05j (2005).
- S12. D. H. Natawidjaja *et al.*, *J. Geophys. Res.*, **109**, B04306 (2004).
- S13. L. Prawirodirdjo *et al.*, *Geophys. Res. Lett.*, **24**, 2601 (1997).
- S14. K. Sieh, S. N. Ward, D. Natawidjaja, B. W. Suwargadi, *Geophys. Res. Lett.*, **26**, 3141 (1999).
- S15. M. Simoes, J. P. Avouac, R. Cattin, P. Henry, *J. Geophys. Res.*, **109**, doi:10.1029/2003JB002958 (2004).
- S16. Earthquake focal mechanisms obtained from the Harvard CMT catalog at <http://www.seismology.harvard.edu/CMTsearch.html>